



Magnetic Fields in M-dwarf Members of the Pleiades Open Cluster Using APOGEE Spectra

Fábio Wanderley¹ , Katia Cunha^{1,2} , Oleg Kochukhov³ , Verne V. Smith⁴ , Diogo Souto⁵ , Lyra Cao⁶ , Kevin Covey⁷ , Steven R. Majewski⁸ , Cintia Martinez⁹ , Philip S. Muirhead^{10,11} , Marc Pinsonneault⁶ , C. Allende Prieto^{12,13} , and Keivan G. Stassun¹⁴

¹ Observatório Nacional/MCTIC, R. Gen. José Cristino, 77, 20921-400, Rio de Janeiro, Brazil; fabiowanderley@on.br

² Steward Observatory, University of Arizona, 933 North Cherry Avenue, Tucson, AZ 85721-0065, USA

³ Department of Physics and Astronomy, Uppsala University, Box 516, S-75120 Uppsala, Sweden

⁴ NSF's NOIRLab, 950 North Cherry Avenue, Tucson, AZ 85719, USA

⁵ Departamento de Física, Universidade Federal de Sergipe, Av. Marcelo Deda Chagas, S/N Cep 49.107-230, São Cristóvão, SE, Brazil

⁶ Department of Astronomy, The Ohio State University, Columbus, OH 43210, USA

⁷ Department of Physics and Astronomy, Western Washington University, Bellingham, WA 98225, USA

⁸ Department of Astronomy, University of Virginia, Charlottesville, VA 22904-4325, USA

⁹ Instituto de Astronomía y Física del Espacio (CONICET-UBA), C.C. 67 Sucursal 28, C1428EHA, Buenos Aires, Argentina

¹⁰ Institute for Astrophysical Research and Department of Astronomy, Boston University, 725 Commonwealth Avenue, Boston, MA 02215, USA

¹¹ Center for Interdisciplinary Exploration and Research in Astrophysics (CIERA) and Department of Physics and Astronomy, Northwestern University, 1800 Sherman Avenue, Evanston, IL 60201, USA

¹² Instituto de Astrofísica de Canarias, E-38205 La Laguna, Tenerife, Spain

¹³ Departamento de Astrofísica, Universidad de La Laguna, E-38206 La Laguna, Tenerife, Spain

¹⁴ Department of Physics and Astronomy, Vanderbilt University, 6301 Stevenson Center Lane, Nashville, TN 37235, USA

Received 2024 March 21; revised 2024 May 13; accepted 2024 June 6; published 2024 August 9

Abstract

Average magnetic field measurements are presented for 62 M-dwarf members of the Pleiades open cluster, derived from Zeeman-enhanced Fe I lines in the H band. A Markov Chain Monte Carlo methodology was employed to model magnetic filling factors using Sloan Digital Sky Survey (SDSS) IV APOGEE high-resolution spectra, along with the radiative transfer code Synmast, MARCS stellar atmosphere models, and the APOGEE Data Release 17 spectral line list. There is a positive correlation between mean magnetic fields and stellar rotation, with slow-rotator stars (Rossby number, $Ro > 0.13$) exhibiting a steeper slope than rapid rotators ($Ro < 0.13$). However, the latter sample still shows a positive trend between Ro and magnetic fields, which is given by $\langle B \rangle = 1604 \times Ro^{-0.20}$. The derived stellar radii when compared with physical isochrones show that, on average, our sample shows radius inflation, with median enhanced radii ranging from +3.0% to +7.0%, depending on the model. There is a positive correlation between magnetic field strength and radius inflation, as well as with stellar spot coverage, correlations which together indicate that stellar spot-filling factors generated by strong magnetic fields might be the mechanism that drives radius inflation in these stars. We also compare our derived magnetic fields with chromospheric emission lines ($H\alpha$, $H\beta$, and Ca II K), as well as with X-ray and $H\alpha$ to bolometric luminosity ratios, and find that stars with higher chromospheric and coronal activity tend to be more magnetic.

Unified Astronomy Thesaurus concepts: Near infrared astronomy (1093); Open star clusters (1160); M dwarf stars (982); Stellar activity (1580); Stellar magnetic fields (1610)

Materials only available in the online version of record: machine-readable table

1. Introduction

Quantitative characterization of magnetic fields provides a deeper understanding of stellar physics. As a star evolves, its stellar wind interacts with the magnetosphere, generating a torque that converts kinetic energy into magnetic energy, reducing the stellar angular momentum and resulting in a slowing of its rotational velocity (Kawaler 1988). This process of magnetic braking over time enables gyrochronology to estimate the age of a star based on its stellar rotation (Skumanich 1972; Barnes 2003), with younger stars tending to have higher magnetic fields and activity than older stars of similar T_{eff} . Another effect caused by magnetic fields is the heating of the stellar chromosphere and coroneae, causing the

emission of, respectively, strong ultraviolet and X-ray nonthermal radiation (Hawley et al. 2014; Astudillo-Defru et al. 2017; Newton et al. 2017).

Magnetic fields are especially important in M-dwarf stars, as these stars have longer spin-down timescales, maintaining magnetic fields for longer periods than hotter stars (Newton et al. 2016). This means that any surrounding exoplanets will experience high-energy fluxes for longer periods, which can impact the habitability of these systems. In addition, since M dwarfs are cool, their habitable zones are located closer when compared to hotter stars, which increases the incident flux, as well as the probability of orbit locking, which, in turn, also impacts habitability. Nonetheless, M-dwarf stars represent around 70% of the stars of our Galaxy (Salpeter 1955; Reid & Gizis 1997), and some of them can live trillions of years on the main sequence, which gives life many opportunities and time to form and evolve around these stars. A deep understanding of their magnetic fields and implications for their



Original content from this work may be used under the terms of the [Creative Commons Attribution 4.0 licence](https://creativecommons.org/licenses/by/4.0/). Any further distribution of this work must maintain attribution to the author(s) and the title of the work, journal citation and DOI.

environment is fundamental for the understanding of these stars and the habitability of their exoplanetary systems.

One method to study stellar magnetic fields is through the Zeeman effect. Magnetically sensitive lines (e.g., having high effective Landé g -factors) are split into components when subject to magnetic fields, which we can observe as an additional line broadening. This broadening scales with the square of the line's central wavelength; therefore, spectral lines located at longer wavelengths are more sensitive to Zeeman splitting than lines with the same effective Landé g -factors located in the bluer part of the spectrum (see Kochukhov 2021, and references therein).

Due to other broadening mechanisms, such as Doppler broadening, stellar rotation, and instrumental broadening, we may not be able to resolve the Zeeman splitting in the spectrum, and what we measure is the Zeeman intensification of an affected line (Basri et al. 1992; Basri & Marcy 1994; Stift & Leone 2003).

There are two main ways to characterize stellar magnetic fields, one considering large-scale and the other small-scale magnetic fields. Large-scale analyses provide a topological view of the stellar magnetic field, separating it into components based on different orientations. The technique used for this characterization, Zeeman–Doppler imaging (ZDI; Kochukhov 2016), is based on the analysis of the circular polarization of the line, described by the Stokes V parameter, and therefore spectro-polarimetric data are needed for this technique. The small-scale magnetic approach models the total intensity of the field and is based on the Stokes I parameter, and no polarimetric stellar data are needed. The review by Kochukhov (2021) discusses the current state of M-dwarf magnetic field studies and presents a compilation of large- and small-scale magnetic field measurements from the literature. Below, we mention the results of a few of these studies.

The first work to model the magnetic field for an M-dwarf star in the literature was Saar & Linsky (1985), who used Ti I lines from a high-resolution ($R \sim 45,000$) K -band spectrum of the flare star AD Leo and found a mean magnetic field of 3.8 kG. Many works followed, modeling the Zeeman effect in M-dwarf spectral lines in the optical and infrared and finding magnetic fields ranging from zero up to 8 kG (Johns-Krull & Valenti 1996; Shulyak et al. 2011, 2014, 2017, 2019; Reiners et al. 2022; Cristofari et al. 2023a, 2023b; Han et al. 2023). Reiners et al. (2022, hereafter R22) determined magnetic fields for a large sample of M dwarfs using CARMENES spectra, and analyzed how magnetic fields are related to parameters such as magnetic flux, activity, and Rossby numbers (Ro), and how these distributions change when comparing the saturated and nonsaturated regimes. Some works studied magnetic fields deriving large-scale magnetic fields from Stokes V , as well as small-scale fields, and found that the latter is considerably greater than the one obtained from circular polarization, which indicates that most of the star's magnetic field is probably stored in small structures at its surface (Phan-Bao et al. 2009; Kochukhov & Lavail 2017; Kochukhov & Shulyak 2019; Kochukhov & Reiners 2020).

All of the studies mentioned above explored magnetic fields in M dwarfs from the Galactic field star population, and these can in principle have different ages and metallicities. Stars from an open cluster, on the contrary, originate from the same molecular cloud and are expected to have approximately the same age and chemistry, making them great benchmarks with which to study stellar evolution and atomic diffusion; but these

are also excellent benchmarks for studying stellar magnetic fields. Because cluster stars form at the same time and share the same chemical composition, metallicity and age dependencies are removed by their intercomparison, and this allows for an investigation of magnetic fields primarily as a function of other stellar properties, such as effective temperatures or rotational periods (Souto et al. 2021). The recent work of Wanderley et al. (2023) used APOGEE near-infrared spectra (Majewski et al. 2017; Abdurro'uf et al. 2022) to derive atmospheric parameters and metallicities, and to study radius inflation in a sample of M-dwarf members of the young Hyades open cluster. Wanderley et al. (2023) found that these stars are on average inflated, and this may be caused by stellar magnetic fields.

In this work, we use spectral lines affected by Zeeman broadening present in the Sloan Digital Sky Survey (SDSS) APOGEE spectra to derive average magnetic fields for a sample of 62 M dwarfs from the young (age = 112 ± 5 Myr; Dahm 2015), near-solar-metallicity (Soderblom et al. 2009) Pleiades open cluster. This is the first study to derive magnetic fields for a sample of M-dwarf members of an open cluster, and also the first to derive magnetic fields for M dwarfs based on APOGEE H -band spectra.

This paper is organized as follows. Section 2 presents the APOGEE data and sample selection. In Section 3, we present the methodology employed to derive average stellar magnetic fields for the Pleiades M-dwarf star sample. In Section 4, we discuss the results, which include the relation between magnetic fields and stellar rotation, comparisons with the literature, radius inflation, and analysis of activity indicators. Finally, Section 5 summarizes our conclusions.

2. APOGEE Data and Sample Selection

We determined average magnetic fields by analyzing near-infrared (1.51 to 1.69 μm), high-resolution (average resolution of $R \sim 22,500$) spectra of Pleiades M-dwarf stars observed by the SDSS-IV APOGEE survey (Blanton et al. 2017; Majewski et al. 2017). As part of SDSS-IV, the APOGEE spectra analyzed here were obtained at the 2.5 m telescope located at the Apache Point Observatory in the Northern Hemisphere (Bowen & Vaughan 1973; Gunn et al. 2006; Wilson et al. 2019).

An initial sample of Pleiades members was obtained from Heyl et al. (2022) and confirmed using the membership analysis in Cantat-Gaudin et al. (2020). We adopted a threshold of 80% of minimum membership probability from Cantat-Gaudin et al. (2020) for a star to be considered a member of the Pleiades. We cross-matched this sample with APOGEE Data Release 17 (DR17; Abdurro'uf et al. 2022) and selected for M dwarfs with $4.7 < M_K < 6.2$ (Mann et al. 2015, 2016), using Two Micron All Sky Survey (2MASS) K_S magnitudes (Skrutskie et al. 2006) and distances from Bailer-Jones et al. (2021). All magnitudes were corrected for extinction using a mean extinction to the Pleiades of $A_V = 0.12$ (Stauffer et al. 2007) and the relations from Wang & Chen (2019). To remove binary stars from the sample, we considered only stars with a scatter in APOGEE radial velocity smaller than 1 km s^{-1} . We also removed stars that presented large Gaia Data Release 3 (DR3; Gaia Collaboration et al. 2023) RUWE numbers ($\text{RUWE} > 1.4$), as this can indicate the presence of an unresolved companion (Belokurov et al. 2020). In addition, stars without a $v_{\text{sin } i}$ measurement in DR17 were also removed from the sample.

We also analyzed the distribution of distances, proper motions (from Gaia DR3), and radial velocities (from

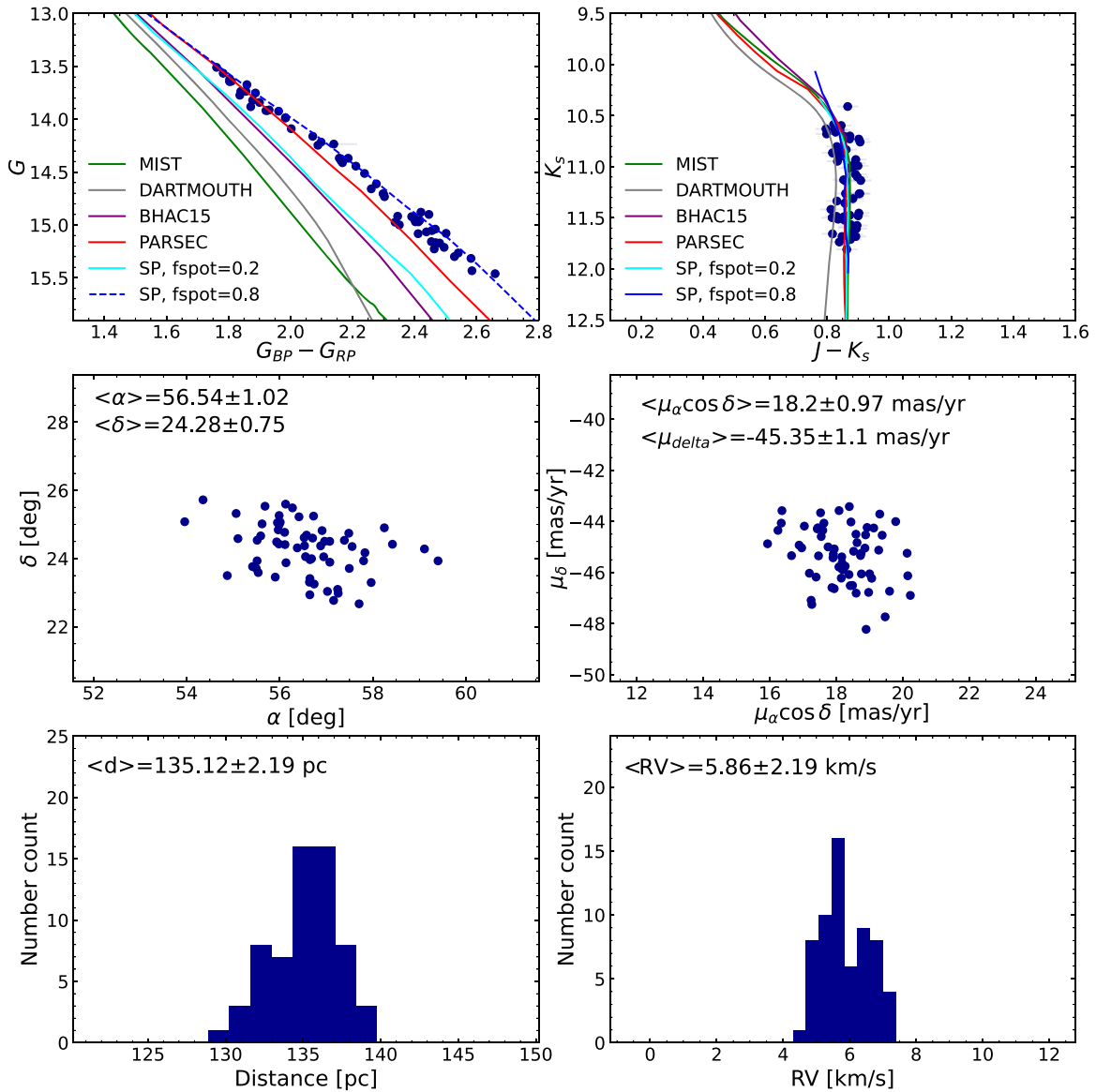


Figure 1. From left to right, the top panels present, respectively, Gaia and 2MASS CMDs; the blue points are the selected M-dwarf members of the Pleiades open cluster. Several 100 Myr solar-metallicity isochrones are shown: MIST, Dartmouth, PARSEC, BHAC15, and SPOTS. Two SPOTS isochrones are shown, one for a photosphere spot coverage of 20% and another for 80%. The middle panels present, respectively, the distribution in space (R.A. and decl.) and proper motions (from Gaia DR3) of the target stars. The bottom panels present, respectively, the distance (Bailer-Jones et al. 2021) and radial velocity histograms. The middle and bottom panels also present the mean and standard deviations for the parameters.

APOGEE DR17) of the selected targets to check for outliers, but we found none. Finally, we also removed from the sample stars that had noisy and problematic APOGEE spectra. Our final sample of Pleiades members analyzed in this study is composed of 62 M dwarfs.

Figure 1 presents the Gaia and 2MASS color–magnitude diagrams (CMDs) of the selected targets (top panels), their distribution in space and proper motions (middle panels), as well as histograms for their star distances (d) and radial velocities (RV) (bottom panels). The average distance, radial velocity, and proper motions along α (R.A.) and δ (decl.) for our Pleiades M-dwarf sample are, respectively: $\langle d \rangle = 135.12 \pm 2.19$ pc, $\langle RV \rangle = 5.86 \pm 2.19$ km s $^{-1}$, $\langle \mu_\alpha \cos \delta \rangle = 18.20 \pm 0.97$ mas yr $^{-1}$ and $\langle \mu_\delta \rangle = -45.35 \pm 1.10$ mas yr $^{-1}$. These results are in good agreement with measurements from Lodieu et al. (2019) of, respectively, 135.15 ± 0.43 pc, 5.67 ± 2.93 km s $^{-1}$, 19.5 mas yr $^{-1}$, and -45.5 mas yr $^{-1}$.

In the top panels of Figure 1, we show several isochrones from the literature: a MIST isochrone (Choi et al. 2016), a Dartmouth isochrone (Dotter et al. 2008), a PARSEC isochrone (Bressan et al. 2012; Nguyen et al. 2022), a BHAC15 isochrone (Baraffe et al. 2015), and two SPOTS isochrones from Somers et al. (2020), one with spots covering 20% of the stellar photosphere and another with a spot coverage of 80%. All isochrones shown are for solar metallicity and an age of 100 Myr, which is roughly the estimated age for the Pleiades open cluster.

The Pleiades study by Covey et al. (2016) found significant scatter in the K versus $J - K_s$ diagram of Pleiades stars (see Figure 3 in their paper). That study also compared the observed colors of Pleiades stars with physical models and found that the $V - K$ colors in rapidly rotating stars present a positive offset for the same V magnitude if compared to slow rotators, which was interpreted as being due to

binarity or a dependency of photospheric/spot properties on rotation rate. The photometric data in the Gaia G versus $G_{BP} - G_{RP}$ CMD, shown in the top-left panel of Figure 1, shows a clear offset, with most isochrones that do not consider stellar spots presenting bluer colors for the same magnitudes, while the SPOTS isochrone associated with an 80% photospheric spot coverage presents an excellent match to the photometric data of the selected stars. We note that this pattern is not seen in the 2MASS CMD, where all isochrones present very small variations, even for different spot fractions, which might be related to the lower photometric spot contrast in the infrared when compared to the visible spectrum.

3. Methodology and Results

To derive average magnetic fields from Zeeman-intensified lines, we used the APOGEE line list (Smith et al. 2021) and model atmospheres from the MARCS grid (Gustafsson et al. 2008). The average magnetic field modeling in this study was done using the Synmast spectral synthesis code (Kochukhov et al. 2010), which computes the effects of magnetic fields on stellar spectra. This code uses polarized radiative transfer calculations to derive $IQUV$ local Stokes parameters for a given magnetic field vector (in radial, meridional, and azimuthal orientations). In this study, we assumed a radial magnetic field and used Synmast to calculate the intensity at seven limb angles. Then another code was used to perform disk integration, converting these intensity fluxes into density fluxes, which can be compared to APOGEE spectra.

To search for the best iron lines in the APOGEE region that can be used as magnetic field indicators for M-dwarf stars, we compared two Synmast syntheses, one computed for 0 kG (i.e., no magnetic field) and another for 3 kG. We selected four Fe I lines as best indicators: 15207.526 Å, 15294.56 Å, 15621.654 Å, and 15631.948 Å. Table 1 presents the selected spectral lines, their central wavelengths in vacuum, the excitation potentials, $\log gf$ values from the APOGEE line list (Smith et al. 2021), effective Landé g -factors collected from the VALD database (Piskunov et al. 1995; Kupka et al. 1999), as well as term designations associated with the upper and lower energy levels. The four selected Fe I lines are considerably sensitive to magnetic fields presenting effective Landé g -factors that range between ~ 1.5 and ~ 1.7 . All the selected Fe I lines except 15621.654 Å are from the same multiple. These lines were used to compute the magnetic fields for all stars in our sample, and gave overall consistent results.

After the selection of diagnostic lines for measuring magnetic fields, the next step in our analysis was to generate a grid of synthetic spectra which was used in the analysis of each star. We adopted the DR17 APOGEE Stellar Parameter and Chemical Abundances Pipeline (ASPCAP; García Pérez et al. 2016; Abdurro'uf et al. 2022) T_{eff} values for each star, along with an approximate $\log g$ (~ 4.7 – 4.8), depending on the stellar T_{eff} . The ASPCAP results used in this work were computed with the Turbospectrum (Plez 2012) code instead of Synspec (Hubeny & Lanz 2011), however we note that there are no significant differences between both sets of results for M dwarfs. The spectra of M dwarfs are relatively insensitive to the microturbulent velocity parameter, as noted by Souto et al. (2017, 2020), who found that a value of 1 km s^{-1} provides good fits to the observations, and we adopt this value in our analysis. All measurable Fe I lines in the APOGEE spectra of M dwarfs have high effective Landé g -factors, which makes them not suitable to be used as rotational broadening indicators. Therefore, we used a sample of OH lines, which are insensitive to magnetic fields. This approach is similar to the one adopted by Johns-Krull et al. (2004), Johns-Krull (2007), Yang et al. (2008), Yang & Johns-Krull (2011), and Lavail et al. (2019), who derived mean magnetic fields for T-Tauri stars from K -band near-infrared spectra, using magnetically insensitive CO lines to measure nonmagnetic broadening. To derive projected rotational velocities ($v \sin i$) for the stars, we used the radiative transfer code Turbospectrum (Plez 2012); we adopted a $v \sin i$ threshold of 3 km s^{-1} given the spectral resolution of the APOGEE spectra. We computed a grid of synthetic spectra, for the adopted stellar parameters for each star and Fe I line, with metallicities ranging from $-0.75 \leq [\text{Fe}/\text{H}] \leq +0.5$ in steps of 0.25, and magnetic field values from 0 to 12 kG in steps of 2 kG, considering only the radial component. We then convolved the synthetic spectra with a rotational profile for the adopted $v \sin i$ as well as a Gaussian profile corresponding to the spectrum line spread function (LSF; see Nidever et al. 2015; Wilson et al. 2019). Each synthesis was fitted to the DR17 normalized APOGEE spectrum (García Pérez et al. 2016) and was subject to small wavelength shifts when needed.

We employed a Markov Chain Monte Carlo (MCMC) method to model the observed spectra and derive magnetic fields for the Pleiades M dwarfs. MCMC is a powerful tool, not only because it provides best fits to observations but also because it gives realistic and well-defined uncertainties based on the posterior distribution. Our methodology considers that the surface of the star can be divided into different components, each associated with a different magnetic field value. The filling factor describes the fraction of the stellar surface associated with a specific $\langle B \rangle$. Many works in the literature have used MCMC to derive average magnetic fields from filling factor determinations

Table 1
Diagnostic Lines

λ (Å)	χ_{exc} (eV)	$\log gf$	Effective Landé g -factor	Lower-level Term Designation	Upper-level Term Designation
15207.526	5.3852	0.067	1.532	LS 3d6.(5D).4s (6D).5 s e7D	LS 3d6.(5D).4s (6D).5p n7D*
15294.560	5.3085	0.523	1.590	LS 3d6.(5D).4s (6D).5 s e7D	LS 3d6.(5D).4s (6D).5p n7D*
15621.654	5.5392	0.280	1.494	LS 3d6.(5D).4s (6D).5 s e5D	LS 3d6.(5D).4s (6D).5p t5D*
15631.948	5.3516	−0.032	1.655	LS 3d6.(5D).4s (6D).5 s e7D	LS 3d6.(5D).4s (6D).5p n7D*

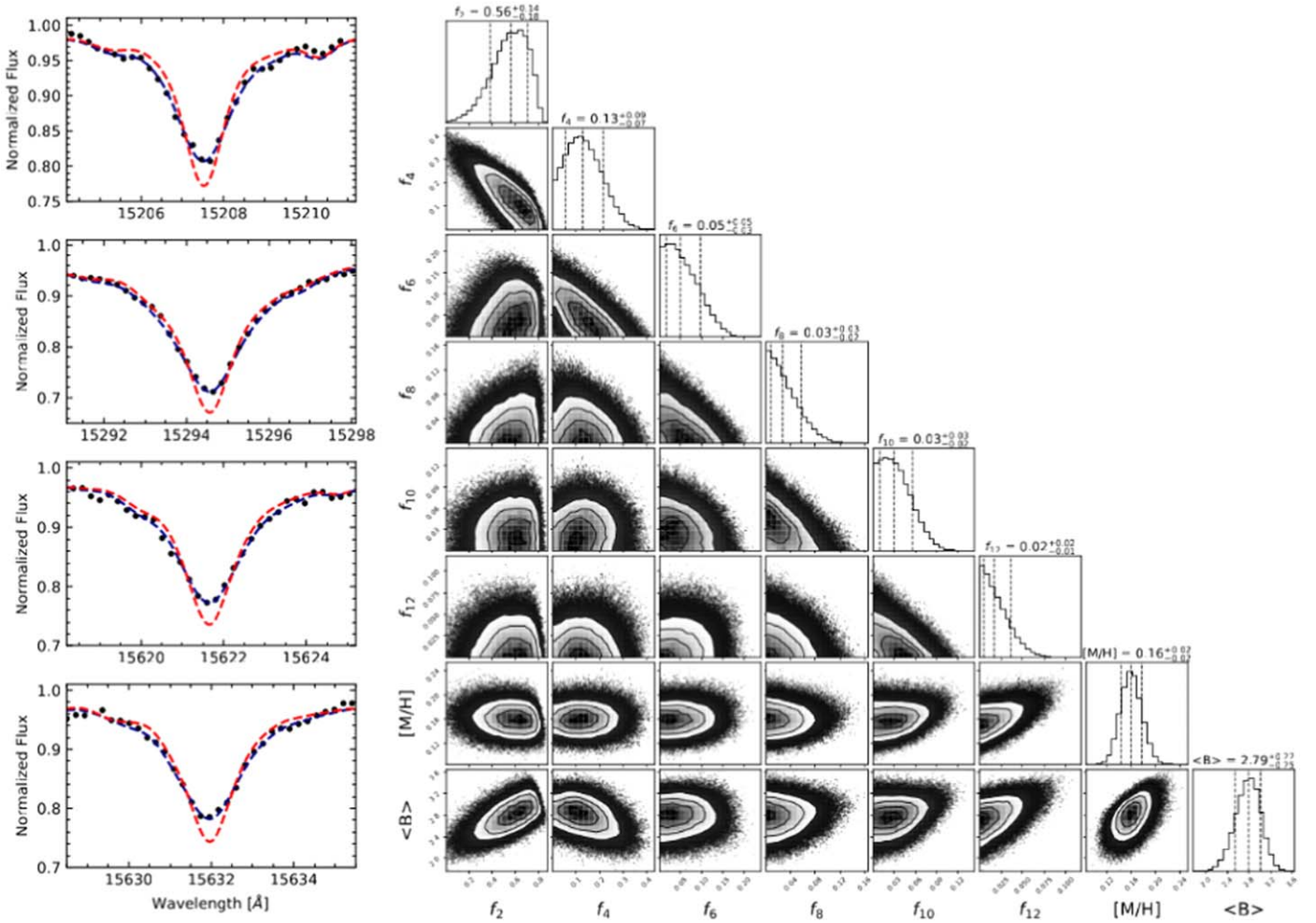


Figure 2. Mean magnetic field results for star 2M03511207+2355575. The left panels show the four Fe I lines used in the modeling; black dots are the observed APOGEE spectrum, red dashed lines are synthetic profiles computed without magnetic field, and dark blue lines are our best fits obtained from the MCMC modeling. The right panel is a corner plot that presents the median and uncertainties (from the 16th and 84th percentiles) of the derived parameters, which includes filling factors associated with magnetic fields from 2 to 12 kG in steps of 2 kG. We also show the obtained average magnetic field (in kilogauss) and its uncertainties.

Table 2
Filling Factors

APOGEE ID	f_0	f_2	f_4	f_6	f_8	f_{10}	f_{12}	$\langle B \rangle$ (G)
2M03420291+2355538	0.218 ± 0.087	0.274 ± 0.152	0.147 ± 0.134	0.034 ± 0.153	0.246 ± 0.22	0.037 ± 0.049	0.044 ± 0.098	4201 ⁵¹¹ ₅₂₉
2M03481801+2353294	0.784 ± 0.058	0.113 ± 0.064	0.037 ± 0.03	0.011 ± 0.011	0.013 ± 0.01	0.005 ± 0.025	0.036 ± 0.016	1032 ²³⁶ ₂₁₅

(Lavail et al. 2019; Kochukhov & Reiners 2020; Hahlin et al. 2021; Hahlin & Kochukhov 2022; R22; Cristofari et al. 2023a, 2023b; Hahlin et al. 2023; Pouilly et al. 2023).

We developed a methodology to derive magnetic fields that employs the python code *emcee* (Foreman-Mackey et al. 2013), and finds the combination of metallicity and six filling factors (associated with magnetic fields of 2–12 kG in a 2 kG step) that best fits the four selected Fe I lines at the same time. We note that the nonmagnetic filling factor f_0 is given by $1 - \sum f_n$. For each entry in the posterior distribution, we calculate an average magnetic field, in gauss units, given by

$$\langle B \rangle = \sum_n f_n \times 1000n, \quad n = [2, 4, 6, 8, 10, 12]. \quad (1)$$

The adopted average magnetic field, along with the lower and upper uncertainties, are given, respectively, by the median,

the 16th, and the 84th percentiles of the posterior distribution. In Table 2, we provide the filling factors and mean magnetic fields for two stars, the ones having the highest and lowest $\langle B \rangle$ in our sample.

In Figure 2, we illustrate the methodology by presenting the best fits, as well as a corner plot for the star 2M03511207+2355575. The left panels show fits for the four lines, where black dots are the observed spectrum, and the blue and red lines represent, respectively, the synthesis with the derived magnetic field and the result with the same metallicity but no magnetic field. The right panel shows the corner plot describing the results. It presents the median and uncertainties (from the 16th and 84th percentiles) of the modeled filling factors and the metallicity. We also show the posterior distribution for the derived average magnetic field.

Table 3
Stellar Data

APOGEE ID	SNR	$v \sin i$ (km s ⁻¹)	T_{eff} (K)	P_{rot} (day)	Ro	$\langle B \rangle$ (G)	$\langle B \rangle/B_{\text{kin}}$	ϕ_B (10 ²⁵ Mx)	$\log(L_X/L_{\text{bol}})$	$\log(L_{\text{H}\alpha}/L_{\text{bol}})$	$\text{EW}_{\text{H}\alpha}$ (Å)	$\text{EW}_{\text{H}\beta}$ Å	$\text{EW}_{\text{Ca II K}}$ Å
2M03420291+2355538	138	17.7	3424	0.89	0.02	4202 ⁺⁵¹¹ ₋₅₃₀	1.52	9.6	... ^a /-2.92 ^b	5.43	-3.74	6	6.55
2M03424379+2532064	103	7.2	3443	3362 ⁺⁶⁶⁹ ₋₆₁₅	1.06	3.81	... ^a /... ^b
2M03515114+2317414	112	13.4	3452	0.87	0.01	3463 ⁺⁵⁸¹ ₋₅₆₇	1.12	4.64	... ^a /... ^b	6.1	-3.68	7.2	...
2M03422864+2501004	131	15.2	3462	1.39	0.02	3850 ⁺⁴⁴⁹ ₋₄₇₈	1.21	4.61	... ^a /-3.13 ^b	5.58	-3.72	9.46	24.76
...

Notes. The complete table is available in electronic format.

^a Wright et al. (2011).

^b Núñez & Agüeros (2016).

(This table is available in its entirety in machine-readable form in the [online article](#).)

The derived mean magnetic fields for the studied Pleiades M-dwarf stars range from ~ 1.0 to ~ 4.2 kG, with a median \pm MAD (median absolute deviation) of 3.0 ± 0.3 kG. Table 3 presents the derived mean magnetic fields for the sample stars, along with the adopted T_{eff} and $v \sin i$, and the signal-to-noise ratios (SNRs) of the analyzed APOGEE spectra. This table also contains some quantities that will be discussed in Section 4: rotational periods, Rossby numbers, ratios between the derived magnetic fields and the magnetic field limit based on kinetic-to-magnetic energy conversion, magnetic fluxes, and activity indicators such as high-energy (X-ray and H α) to bolometric luminosity ratios and H α , H β , and Ca II K equivalent widths.

4. Discussion

4.1. Magnetic Fields, Rossby Numbers, and Stellar Rotation

We collected rotational periods for 53 stars in our sample from the works by Hartman et al. (2010), Rebull et al. (2016), and Covey et al. (2016), who analyzed data from the HATNet (Bakos et al. 2004), K2 (Howell et al. 2014), and PTF (Law et al. 2009; Rau et al. 2009) surveys, respectively. The rotational periods of the sample stars include both slow and rapid rotators, encompassing rotational periods ~ 0.7 –17.3 days.

The Rossby number (Ro) is an important indicator of stellar activity, and is given by the ratio between the rotational period and the convective turnover time. The convective turnover time, τ , is defined as the time that it takes a convective cell to traverse the convective envelope of a star. Due to both their deeper convective envelopes and slower convective velocities, cooler stars are expected to have longer convective turnover times, and also to be able to sustain dynamos longer than hotter stars. For τ , measured in units of days, we used the relation $\tau = 12.3 \times (L/L_{\odot})^{-0.5}$, derived by R22. Bolometric luminosities were determined using distances from Bailer-Jones et al. (2021), 2MASS K_s magnitudes, and bolometric corrections from photometric calibrations from Mann et al. (2015, 2016). This calibration is based on 2MASS J - and V -band magnitudes collected from Stauffer et al. (2007), Lasker et al. (2008), Zacharias et al. (2012), and Muirhead et al. (2018). We also employed the same method to account for extinction described in Section 2.

The mean magnetic fields derived for the sample stars versus their projected rotational velocities, $v \sin i$ (both of which are quantities derived from the APOGEE spectra), are shown in Figure 3 as blue symbols. The blue circles represent stars for which we can estimate the $v \sin i$, while the blue triangles are stars having $v \sin i$ values up to 3 km s^{-1} , the adopted threshold in $v \sin i$ that can be estimated in this study. We also show in this figure literature results from R22 as black \times 's. The mean magnetic fields for the Pleiades stars generally overlap with the M dwarfs in R22 within the overlapping $v \sin i$ range, showing just a small systematic difference in $\langle B \rangle$ when compared to R22.

Figure 4 shows our results for magnetic fields versus rotational periods for the Pleiades M dwarfs (red and blue open circles), along with results from the literature for comparison. We compiled a total of 281 average magnetic field measurements from the literature. The results from Shulyak et al. (2017) and Shulyak et al. (2019) are represented by green squares in the figure. Results from Cristofari et al. (2023a) and Cristofari et al. (2023b) are represented by cyan diamonds. Results from R22 are for stars with $T_{\text{eff}} < 4000$ K and are represented by black \times 's. Finally, other results from the literature (orange triangles) are from the following works: Saar & Linsky (1985), Saar (1994),

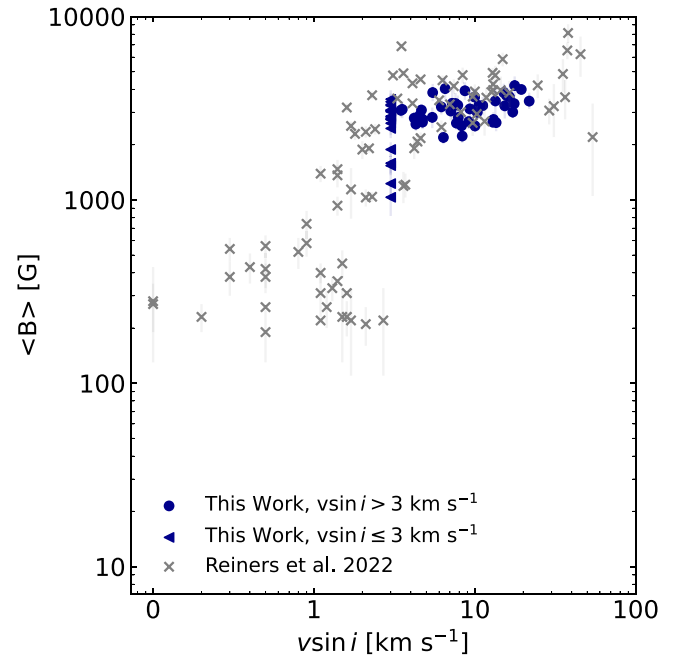


Figure 3. Distribution of the derived average magnetic fields vs. adopted projected rotational velocities, $v \sin i$, for the studied M dwarfs in the Pleiades are represented by blue circles and triangles for, respectively, stars with $v \sin i > 3 \text{ km s}^{-1}$ and with $v \sin i \leq 3 \text{ km s}^{-1}$. Results from R22 are also shown (black \times 's).

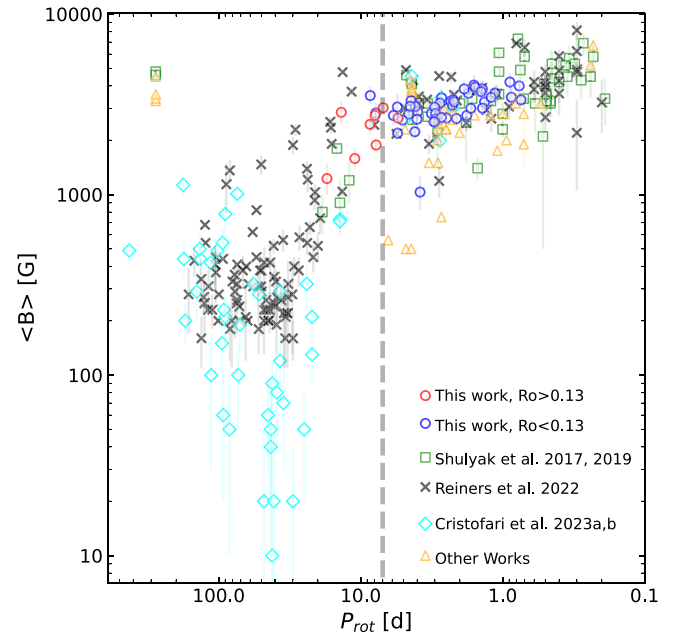


Figure 4. Mean magnetic fields vs. rotational periods for Pleiades M-dwarf rapid (open blue circles, $\text{Ro} < 0.13$) and slow rotators (open red circles, $\text{Ro} > 0.13$), along with data compiled from the literature. Green squares, black \times 's, and cyan diamonds are data from, respectively, Shulyak et al. (2017, 2019), R22, and Cristofari et al. (2023a, 2023b). Orange triangles show results from other works; see text for references.

Johns-Krull & Valenti (1996), Saar (1996), Johns-Krull & Valenti (2000), Kochukhov et al. (2001), Afram et al. (2009), Kochukhov et al. (2009), Phan-Bao et al. (2009), Shulyak et al. (2011, 2014), Kochukhov & Lavail (2017), and Kochukhov & Shulyak (2019).

We can divide the $\langle B \rangle$ – P_{rot} plane in Figure 4 into two regions that correspond to the saturated and unsaturated regimes. Red

and blue open circles in this figure represent, respectively, stars in our sample that are slow rotators ($Ro > 0.13$, nonsaturated regime) and rapid rotators ($Ro < 0.13$, saturated regime). We added a vertical dashed line at $P_{\text{rot}} = 7$ days to Figure 4, which is an estimated threshold analogous to the separation based on Rossby numbers. Stars in the nonsaturated regime are expected to have lower activity levels and also to present a greater dependency between Rossby numbers and magnetic fields. Stars in the saturated regime are in the limit of kinetic-to-magnetic energy conversion, and show a much flatter relation, although there is still some dependency between Rossby numbers and magnetic fields.

Most of the stars in our sample have rotational periods roughly between 1 and 10 days. Overall, stars in the saturated regime (blue open circles) follow an approximately constant $\langle B \rangle$ as a function of P_{rot} , showing just a modest inclination in the trend. It is clear that our results for this population overlap with results from the literature in this regime. For sample stars in the unsaturated regime (open red circles), $\langle B \rangle$ values begin to show a desaturation signal (at $P_{\text{rot}} \sim 7$ days), with the slowest rotating stars of our sample presenting a steeper negative relation between rotational periods and magnetic fields than for faster rotators. Although our sample does not include very slowly rotating stars, our results generally overlap with literature values and are in line with the steep relation between magnetic fields and rotational periods in the literature, which extends to $P_{\text{rot}} \sim 100$ days. It is interesting to note that, despite the fact that our sample and that from R22 both have the same upper T_{eff} limit of 4000 K, the latter sample reaches much greater rotational periods and lower magnetic fields. The possible main reason for this is that the R22 results are for field M dwarfs, while our work considers only M-dwarf star members of the very young Pleiades open cluster. M dwarfs from the field may have had much more time to lose their magnetic fields and angular momentum when compared to the young stars from our sample.

The dependency between rotation and magnetic fields can be explained by the dynamo mechanism that converts kinetic into magnetic energy. The total magnetic field of the star is limited by its available kinetic energy, and this maximum magnetic field is denoted as B_{kin} . Here, we adopt the relation from Reiners et al. (2009) for B_{kin} (in units of gauss):

$$B_{\text{kin}} = 4800 \times \left(\frac{ML^2}{R^7} \right)^{1/6}, \quad (2)$$

where L is the derived luminosity (in L_{\odot} units), M is the stellar mass (in M_{\odot} units), and R is the radius (in R_{\odot} units) derived using the Stefan–Boltzmann equation, with the adopted T_{eff} . We derived magnetic fluxes (ϕ_B) by multiplying the obtained average magnetic field by $4\pi R^2$. Masses were determined from isochrones, following the methodology discussed in Wanderley et al. (2023). In summary, we selected SPOTS isochrones from Somers et al. (2020) for 100 Myr and solar metallicity, interpolated isochrones associated with different photospheric spots fractions (f_{spots}), and adopted as the mass of the star the point in the interpolated isochrone plane with the closest T_{eff} and luminosity of the star.

We also estimated masses using Dartmouth (Dotter et al. 2008), MIST (Choi et al. 2016), and BHAC15 (Baraffe et al. 2015) isochrones, and found that, as expected, the choice of isochrone does not significantly change the B_{kin} results.

Figure 5 presents our results for $\langle B \rangle$ as a function of Rossby number (left panel), $\langle B \rangle/B_{\text{kin}}$ as a function of rotational period (middle panel), and ϕ_B as a function of rotational period (right panel). Stars with $Ro > 0.13$ are represented by open red circles, and stars with $Ro < 0.13$ are represented by open blue circles. The gray dashed vertical line in the left panel at $Ro = 0.13$ is the threshold that corresponds to the separation between the saturated and the nonsaturated regimes.

For stars in the saturated regime in our sample (open blue circles), we derived relations between their mean magnetic fields with Rossby numbers, and between $\langle B \rangle/B_{\text{kin}}$ and ϕ_B with rotational periods by using nonlinear least squares to fit power-law functions. The obtained relations are found below, and are shown as solid blue lines in Figure 5:

$$\langle B \rangle = 1604G \times Ro^{-0.20}, \quad (3)$$

$$\langle B \rangle/B_{\text{kin}} = 1.13 \times P_{\text{rot}}^{-0.21}, \quad (4)$$

$$\phi_B = 6.01 \times 10^{25} \text{Mx} \times P_{\text{rot}}^{-0.23}. \quad (5)$$

For comparison, we also show in Figure 5 similar relations derived by R22 for their sample of rapid and slow rotators (represented by cyan and red dashed lines, respectively).

As previously discussed in Figure 4, the results in the left panel of Figure 5 show a clear difference in the trends between the saturated and unsaturated regimes. The relation obtained here for the saturated stars (Equation (3)) is less steep than for the unsaturated ones and similar to the one derived in R22. Given the small number of slow-rotating stars and small range in Rossby number of our sample, we did not compute a best-fit relation for the unsaturated stars, but the comparison of our results (open red circles) with the relation in R22 (red dashed line) shows good agreement. The results in the middle panel of Figure 5 show that, overall, most of our stars present $\langle B \rangle/B_{\text{kin}}$ ratios near 1 (represented by the gray horizontal dashed line), indicating that they are near the peak of magnetic energy production based on their available kinetic energy. There is a small trend with rotational period (or Rossby number), showing an inverse correlation between $\langle B \rangle/B_{\text{kin}}$ and rotational period. This is illustrated by our derived relation for rapid rotators (Equation (4)), which is very similar to the one derived by R22 (dashed blue line), presenting a similar slope, and being almost the same as our relation. The results in the right panel of Figure 5 show an overall similar behavior as found for $\langle B \rangle$ versus Rossby number, with saturated stars presenting a smaller dependency with P_{rot} than nonsaturated ones. This is illustrated by the blue solid line showing the relation between magnetic flux and rotational period for the rapid rotator sample (Equation (5)). The well-defined relation obtained here for the saturated regime for the Pleiades M dwarfs is different from the results in R22, who found a large scatter in magnetic flux for fast-rotating stars and without a well-defined relation. Such difference in the results may come from the fact that R22 studied field stars with different ages, while our sample has a well-constrained age of ~ 100 million years, and the well-defined trend for the saturated regime may be an indication of a strong connection between magnetic flux and stellar age. The rotational periods and computed Rossby numbers, magnetic fluxes, and $\langle B \rangle/B_{\text{kin}}$ for the stars are presented in Table 3.

4.2. Radius Inflation in the Pleiades M Dwarfs

Several works in the literature have compared stellar radii measurements with predicted radii from stellar isochrones that

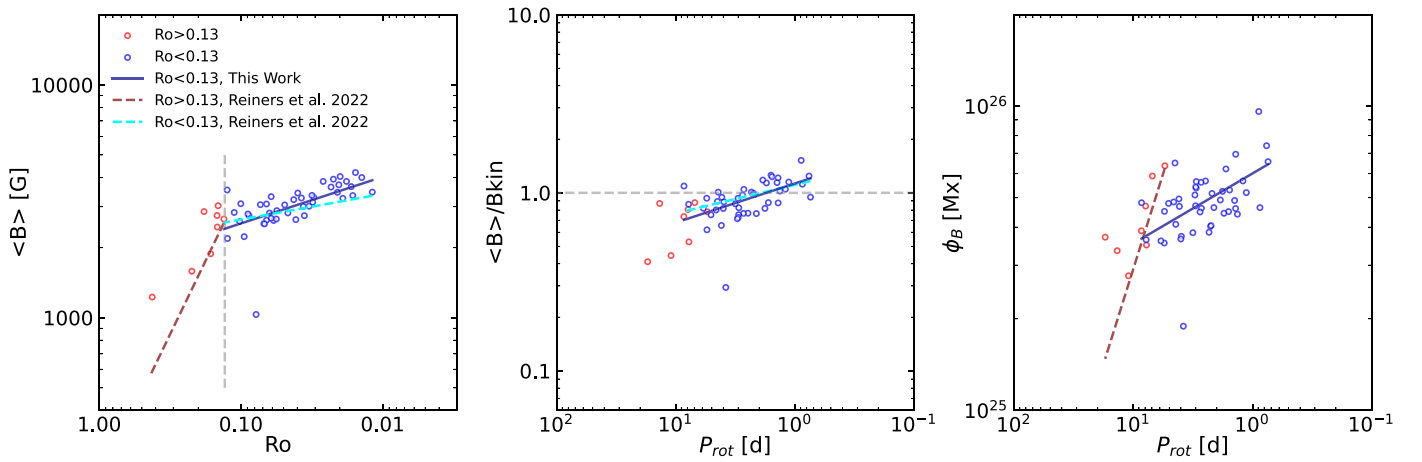


Figure 5. Comparison of different magnetic field indicators as a function of Rossby number (left panel) and rotational period (middle and right panels). Stars with $Ro < 0.13$ are represented by open blue circles, and stars with $Ro > 0.13$ are represented by open red circles. The left panel presents the distribution of the obtained magnetic fields, the middle panel presents the ratio between the obtained average magnetic fields and the magnetic field limit based on the stellar kinetic energy, and the right panel presents the magnetic flux of the stars. The left panel shows a vertical gray line to represent $Ro = 0.13$. The horizontal gray line in the middle panel represents the point where the magnetic field is at its maximum physical limit, based on kinetic-to-magnetic energy conversion, where $\langle B \rangle = B_{kin}$. We also show relations between rotational and magnetic parameters derived by this work (solid lines) and R22 (dashed lines), for slow (red lines) and/or rapid rotators (cyan lines).

do not include magnetic fields, and have found that stars, M-dwarf stars in particular, have larger radii than predicted by the models (Reiners et al. 2012; Jackson et al. 2016, 2018; Jeffers et al. 2018; Kesseli et al. 2018; Jackson et al. 2019; Jaehrig et al. 2019; Wanderley et al. 2023). Stellar magnetic fields can have the effect of decreasing convective efficiency and/or generating stellar spots, which reduces the stellar photospheric temperature and causes the star to inflate (Chabrier et al. 2007). The term “radius inflation” (R_{frac} , fractional radius inflation) refers to the fractional difference between the radius obtained from measurements and isochrone models (R_{iso}).

In this study, we follow the same methodology as discussed in Wanderley et al. (2023) to measure radius inflation for our sample of Pleiades M dwarfs, using as baseline MIST, Dartmouth, and BHAC15 isochrones with solar metallicities and ages of 100 Myr. As discussed in Section 4.1, stellar radii were derived from the Stefan–Boltzmann equation, using adopted T_{eff} along with luminosities derived from photometric relations. The median \pm MAD radius inflation obtained in this work is $7.0 \pm 1.5\%$, $6.5 \pm 1.4\%$, and $5.4 \pm 1.3\%$, respectively, based upon the MIST, Dartmouth, and BHAC15 isochrones. The median radius inflation of $\sim 5\%$ – 7% found here for the Pleiades M dwarfs is considerably larger than the median radius inflation of $\sim 2\%$ that was obtained by Wanderley et al. (2023) for M-dwarf members of the older (age = 625 ± 50 Myr; Perryman et al. 1998) Hyades open cluster. Greater radius inflation for younger M dwarfs is generally in line with expectations from gyrochronology, that stars from younger clusters should present higher average magnetic fields if compared to older stars with the same masses. It should be kept in mind, however, that while the sample of Wanderley et al. (2023) included M dwarfs beyond the fully convective threshold, our Pleiades sample is composed only of partially convective M dwarfs, and models including magnetic fields predict that radius inflation can be inhibited in fully convective stars (Feiden et al. 2015).

In addition, in this study we also computed radius inflation using as a baseline SPOTS isochrone models from Somers et al. (2020). These models consider that stellar spots change

the internal structure of the star by suppressing convection, reducing the photospheric temperature, and as a consequence inflating the star. As previously, to derive the fractional radius inflation (R_{frac}) and photospheric spot fractions (f_{spots}), we adopted SPOTS isochrones for solar metallicity, an age of 100 Myr, and the same methodology to measure radius inflation as presented in Wanderley et al. (2023). (We refer to this previous study for details.)

Using SPOTS models, we find a median radius inflation for our sample of $3.0\% \pm 1.2\%$, which is smaller when compared to that obtained with either the MIST, Dartmouth, or BHAC15 isochrones. Less radius inflation is expected when using the Somers et al. (2020) isochrones as a baseline due to the decrease in luminosity for more spotted models. The median radius inflation found here for the Pleiades M dwarfs is larger than the median radius inflation of $1.0\% \pm 0.5\%$ reported by Wanderley et al. (2023) for the Hyades.

Figure 6 presents our results for the mean magnetic fields and derived radius inflation (R_{frac}) for the sample M dwarfs. Panels, from left to right, show the radius inflation for the MIST, Dartmouth, BHAC15, and SPOTS isochrones. The main result from all panels is that, overall, Pleiades M dwarfs having higher mean magnetic fields have more inflated radii. The work of Feiden et al. (2015) applied modifications in the Dartmouth models to include the effects of magnetic fields, and found a positive correlation between magnetic field strength and radius inflation when considering either rotational or turbulent dynamos. This finding agrees with our results, as for all studied isochrones stars with higher magnetic fields tend to be more inflated. There is, however, a tendency for $\langle B \rangle$ to have a weaker dependency with radius inflation, in particular for the SPOTS models with R_{frac} between 0.02 and 0.10. Figure 7 presents the derived photospheric stellar spot fractions as a function of average magnetic fields. For the majority of the Pleiades M dwarfs, there is a positive correlation between stellar spot fractions and magnetic field, although with a small number of outliers. Finally, we note that there is one clear outlier star in Figures 6 and 7, having high radius inflation and low $\langle B \rangle$. This star has the lowest K_s magnitude from our sample (K_s mag = 10.42; Skrutskie et al. 2006). Its position in the K_s

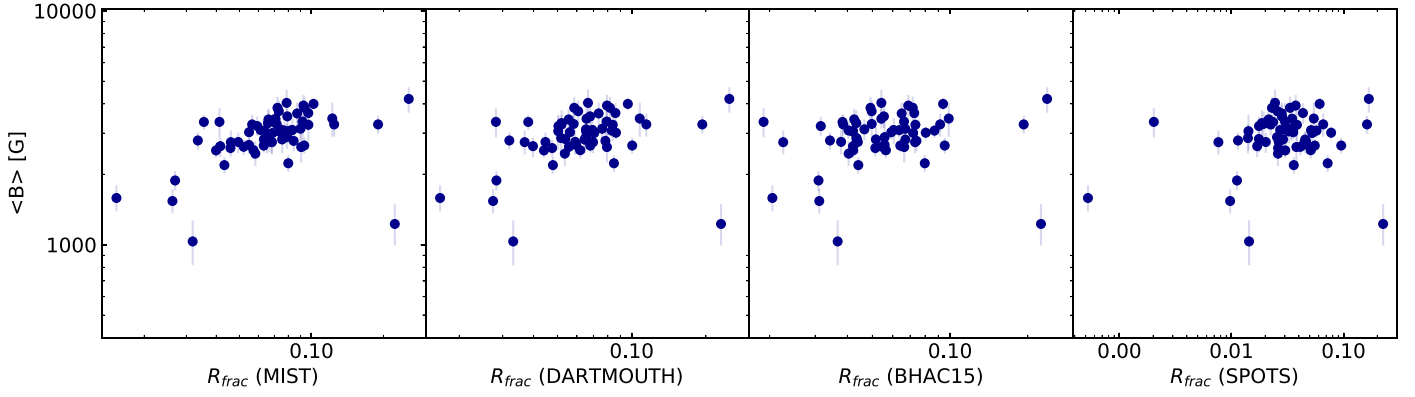


Figure 6. Derived average magnetic fields and radius inflation for the sample of 62 stars, considering different sets of isochrones. From left to right, radius inflation is based on, respectively, MIST, Dartmouth, BHAC15, and SPOTS isochrones.

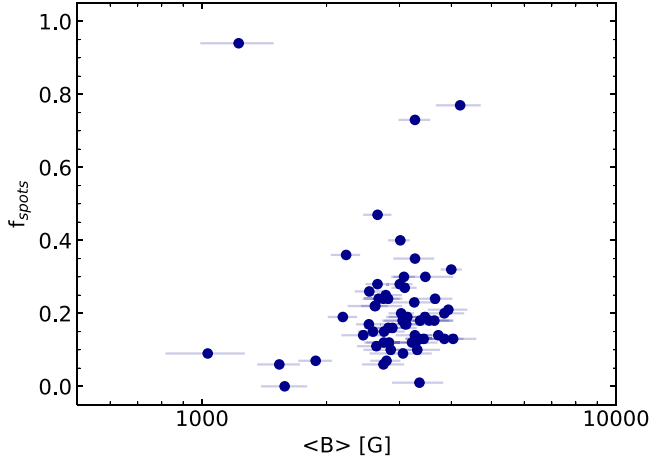


Figure 7. Fractional stellar photospheric spots coverage from SPOTS models (Somers et al. 2020) as a function of our derived average magnetic fields.

versus $J-K_s$ diagram (see Figure 1) might hint that it is not a member of the Pleiades cluster. However, this star was found in Cantat-Gaudin et al. (2020) to have a 100% probability of being a member of the Pleiades. Note that our f_{spots} may progressively increase for $\langle B \rangle$ larger than roughly 2500 G. Although, Cao & Pinsonneault (2022) previously found constant f_{spots} at low Rossby number ($\text{Ro} < 0.21$) in their analysis of Pleiades dwarfs, with their values of f_{spots} modeled from a two-component surface defined by a starspot filling factor and a starspot temperature contrast.

4.3. Magnetic Fields and Activity

Stellar activity is a term for the phenomenon of stellar variability, which is mainly a consequence of strong magnetic fields. Stellar variability can be caused by stellar spots, which are temporary cooler regions in the stellar photosphere where the strong magnetic fields suppress convection. As the star rotates these cold spots can reduce the observed stellar flux, and result in periodic changes in the magnitude of the star. Another important mechanism that can generate stellar variability is high-energy nonthermal emission. Strong magnetic fields are responsible for heating the coronae and chromosphere of active stars, which results in considerably larger amounts of high-energy radiation emission than expected from their blackbody profiles. Heating of the coronae results in an excess in the X-ray stellar output that can be measured as the ratio between the X-ray and bolometric luminosity, while heating of the

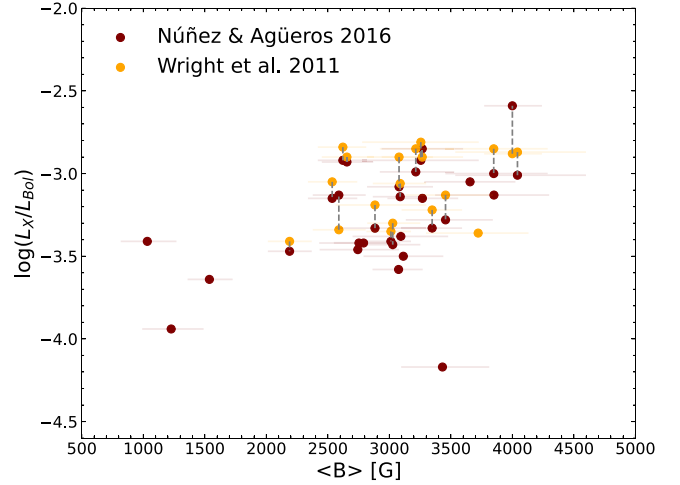


Figure 8. Derived average magnetic fields as a function of the ratios between X-ray to bolometric luminosities for stars of our sample in common with the study of Wright et al. (2011, orange circles) and Núñez & Agüeros (2016, maroon circles). The same stars are connected by dashed lines.

chromosphere is often studied from magnetically sensitive emission lines, such as $H\alpha$, $H\beta$, and the Ca II H and K lines. Since coronal and chromospheric nonthermal emissions are produced by the effect of stellar magnetic fields, they are also variable, and change according to the stellar magnetic cycle.

To study the relation between activity and magnetic fields in the Pleiades M dwarfs, we cross-matched our sample with the targets in the X-ray studies of Núñez & Agüeros (2016) and Wright et al. (2011), and found 31 stars in common with the first study (not considering 17 stars having only upper limit measurements), and 19 stars in common with the latter study; the X-ray to bolometric luminosity ratios in those works are X-ray flux measurements from Einstein and ROSAT observations (Micela et al. 1990; Stauffer et al. 1994; Micela et al. 1996, 1999; Stelzer et al. 2000). The results are summarized in the top panel of Figure 8, where we show the logarithm of the X-ray to bolometric luminosity ratios versus our derived magnetic fields. There is a clear correlation between the two variables, with a Pearson correlation coefficient of 0.46 for the sample in Núñez & Agüeros (2016, shown as maroon circles) and 0.35 for the sample in Wright et al. (2011, shown as orange circles), indicating that stars with stronger magnetic fields tend to present greater X-ray to bolometric luminosity ratios.

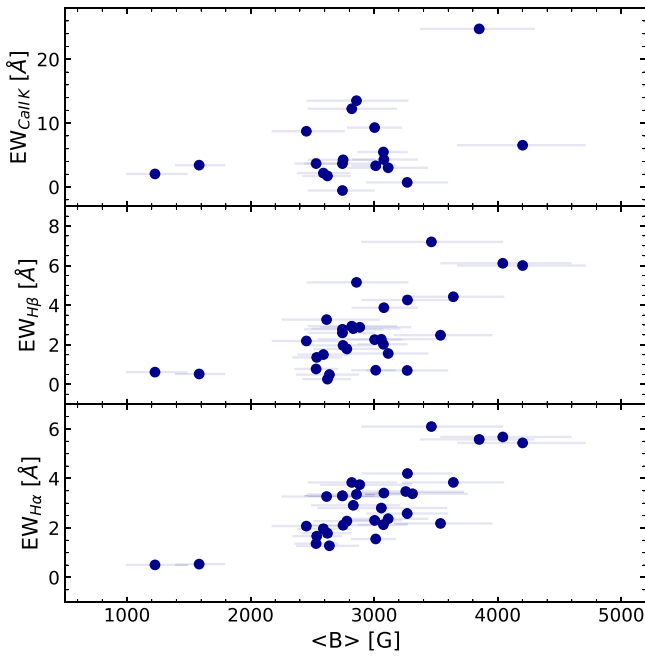


Figure 9. Derived average magnetic fields as a function of the equivalent widths of magnetically sensitive chromospheric emission lines for stars of our sample that are in common with the work of Fang et al. (2018). The panels present, from top to bottom, the Ca II K, H β , and H α emission lines.

Concerning chromospheric activity, the work of Fang et al. (2018) measured equivalent widths for H α , H β , and Ca II K emission lines for stars in open clusters using LAMOST Data Release 3 spectra (Cui et al. 2012). We cross-matched our Pleiades sample with their database and found 33 stars in common with measured H α , 31 with measured H β , and 19 with measured Ca II K. The three panels in Figure 9 present our derived average magnetic field measurements versus the total equivalent width for the Ca II K line (top panel), H β (middle panel), and H α (bottom panel), where all equivalent widths are in units of angstrom. Similar to what was found for the X-ray to bolometric ratios, there is a correlation between the mean magnetic fields for the Pleiades M dwarfs and the equivalent widths of the emission lines for all three lines, although the results for the Ca II K line are less clear.

Figure 10 shows the H α to bolometric luminosity ratios as a function of mean magnetic fields for stars in our sample having H α emission strength measurements ($EW_{H\alpha}$) reported in Table 3. To convert H α equivalent widths into $L_{H\alpha}/L_{bol}$, we employed the methodology described in Stassun et al. (2012). Similar to what is seen for the relation between $EW_{H\alpha}$ and $\langle B \rangle$ (bottom panel of Figure 9), there is a clear correlation between the H α to bolometric luminosity ratios and the derived magnetic fields, with a Pearson correlation coefficient of 0.78.

Overall, it is reassuring that in this study we find that the more magnetic stars in our sample tend also to be more active, based on our magnetic field measurements and independent results from activity indicators from other works in the literature. The X-ray and H α to bolometric luminosity ratios as well as the equivalent widths for the H α , H β , and Ca II K emission lines of the stars are presented in Table 3.

5. Conclusions

We used the Synmast code (Kochukhov et al. 2010), along with a MCMC methodology, to compute synthetic spectra and

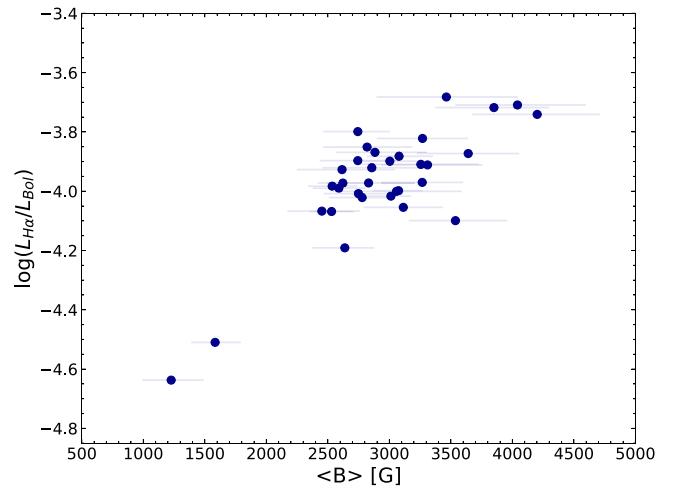


Figure 10. Derived average magnetic fields as a function of H α to bolometric luminosities. We employed the methodology described in Stassun et al. (2012) to convert H α equivalent widths (taken from Fang et al. 2018) into $L_{H\alpha}/L_{bol}$.

analyze magnetically sensitive Fe I lines to derive average magnetic fields for 62 M-dwarf members of the young (age = 112 ± 5 Myr; Dahm 2015) and nearby Pleiades open cluster. This analysis is based on the SDSS-IV APOGEE spectra (Majewski et al. 2017; Abdurro'uf et al. 2022), the APOGEE line list (Smith et al. 2021), effective Landé g-factors from the VALD database (Piskunov et al. 1995; Kupka et al. 1999), and model atmospheres from the MARCS grid (Gustafsson et al. 2008).

A search was carried out to find the best Fe I lines in the APOGEE spectral region that were sensitive to Zeeman broadening and which could be used as diagnostic lines for measuring mean magnetic fields in M dwarfs, with four Fe I lines identified and selected as the best indicators: 15207.526 Å, 15294.56 Å, 15621.654 Å, and 15631.948 Å. The derived mean magnetic fields for the studied Pleiades M-dwarf stars range from ~ 1.0 to ~ 4.2 kG, with a median \pm MAD of 3.0 ± 0.3 kG, not reaching the lowest magnetic field and rotation levels reported in other studies that explored field stars of similar masses, which is probably explained by the young age of the cluster.

The derived mean magnetic field measurements in the Pleiades M dwarfs were used to study correlations with Rossby number (Ro) and stellar rotation. The Rossby number is given by the ratio between the rotational period and the convective turnover time, being an important indicator of stellar activity. We find a clear trend that more magnetic stars have, on average, higher projected rotational velocities, $v \sin i$. The Rossby number was used to separate our sample into rapid ($Ro < 0.13$) and slow rotators ($Ro > 0.13$). Overall, our results for $\langle B \rangle$ versus P_{rot} and B versus Rossby number overlap with results from the literature for field stars, and indicate that the population of stars with $Ro < 0.13$ exhibit a steeper relation between magnetic field and rotational period or Rossby number when compared to stars with $Ro > 0.13$. However, even for $Ro > 0.13$, there remains a shallow trend between Rossby number and magnetic field, which is given by $\langle B \rangle = 1604 \times Ro^{-0.20}$.

For this sample of Pleiades M dwarfs, we also investigated the ratio between mean magnetic field and the maximum magnetic field limit ($\langle B \rangle/B_{kin}$) that is reached based on kinetic-to-magnetic energy conversion. It is found that most of the

studied Pleiades M dwarfs are at the limit of kinetic-to-magnetic energy conversion, or are in the saturated regime, having $\langle B \rangle / B_{\text{kin}} \approx 1$. Unlike previous results in the literature for field stars in the saturated regime, the computed stellar magnetic fluxes ϕ_B as a function of P_{rot} for the Pleiades M dwarfs show similar trends obtained for $\langle B \rangle$ versus P_{rot} .

Another important effect of magnetic fields is to inflate the stellar radii of cool dwarfs. Radius inflation corresponds to the fractional difference (R_{frac}) between the radius obtained from measurements and predictions from isochrone models. In this study, we derived the radii for the studied M dwarfs and used MIST, Dartmouth, BHAC15, and SPOTS isochrones as baselines to infer their radius inflation. We obtain a median \pm MAD radius inflation for our sample of $7.0\% \pm 1.5\%$, $6.5\% \pm 1.4\%$, $5.4\% \pm 1.3\%$, and $3.0\% \pm 1.2\%$, respectively, being more inflated than M dwarfs in the older Hyades open cluster (Wanderley et al. 2023). For the Pleiades, it is noticeable that for SPOTS isochrones there is less radius inflation when compared to nonspotted isochrones, as expected. In addition, our results indicate that more magnetic stars have more inflated radii, showing a correlation between R_{frac} and $\langle B \rangle$. For SPOTS models in particular, there is, however, a tendency for $\langle B \rangle$ to exhibit a weaker dependency with radius inflation for R_{frac} between 0.02 and 0.10. For the majority of the Pleiades M dwarfs in our sample, there is a positive correlation between stellar spot fraction and magnetic field, although with a small number of outliers.

To study the relation between chromospheric stellar activity and magnetic fields in the Pleiades M dwarfs, we compared our derived mean magnetic fields with high-energy nonthermal emission indicators, such as equivalent-width measurements of the $H\alpha$, $H\beta$, and Ca II K lines, as well as $H\alpha$ to bolometric luminosity ratios. For all of these, we find a positive correlation between chromospheric activity and magnetic fields. A positive correlation was also obtained between the mean magnetic field and the ratio between X-ray to bolometric luminosity, which is an important indicator of coronal activity. Overall, it is reassuring that the more magnetic stars in this study also tend to be more active, and this is based on our magnetic field measurements from APOGEE spectra, which is independent of the results for activity indicators obtained from the literature. This study opens a new window into using the APOGEE survey to investigate magnetic fields in cool stars.

Acknowledgments

We thank the referee for the comments that improved the paper. F.W. acknowledges support from a fellowship by Coordenação de Ensino Superior—CAPES. K.C. and V.S. acknowledge that their work is supported, in part, by the National Science Foundation through NSF grant AST-2009507. O.K. acknowledges support by the Swedish Research Council (grant agreement Nos. 2019-03548 and 2023-03667), the Swedish National Space Agency, and the Royal Swedish Academy of Sciences. D.S. thanks the National Council for Scientific and Technological Development—CNPq.














Funding for the Sloan Digital Sky Survey IV has been provided by the Alfred P. Sloan Foundation, the U.S. Department of Energy Office of Science, and the Participating Institutions. SDSS-IV acknowledges support and resources from the Center for High-Performance Computing at the University of Utah. The SDSS website is www.sdss.org. SDSS-IV is managed by the Astrophysical Research consortium for the Participating

Institutions of the SDSS Collaboration including the Brazilian Participation Group, the Carnegie Institution for Science, Carnegie Mellon University, the Chilean Participation Group, the French Participation Group, the Harvard-Smithsonian Center for Astrophysics, the Instituto de Astrofísica de Canarias, The Johns Hopkins University, the Kavli Institute for the Physics and Mathematics of the Universe (IPMU)/University of Tokyo, the Lawrence Berkeley National Laboratory, the Leibniz Institut für Astrophysik Potsdam (AIP), Max-Planck-Institut für Astronomie (MPIA Heidelberg), Max-Planck-Institut für Astrophysik (MPA Garching), Max-Planck-Institut für Extraterrestrische Physik (MPE), the National Astronomical Observatory of China, New Mexico State University, New York University, University of Notre Dame, Observatório Nacional / MCTI, The Ohio State University, Pennsylvania State University, Shanghai Astronomical Observatory, United Kingdom Participation Group, Universidad Nacional Autónoma de México, University of Arizona, University of Colorado Boulder, University of Oxford, University of Portsmouth, University of Utah, University of Virginia, University of Washington, University of Wisconsin, Vanderbilt University, and Yale University.

Facility: Sloan

Software: Matplotlib (Hunter 2007), Numpy (Harris et al. 2020), Synmast (Kochukhov et al. 2010), Turbospectrum (Plez 2012).

ORCID iDs

Fábio Wanderley  <https://orcid.org/0000-0003-0697-2209>
 Katia Cunha  <https://orcid.org/0000-0001-6476-0576>
 Oleg Kochukhov  <https://orcid.org/0000-0003-3061-4591>
 Verne V. Smith  <https://orcid.org/0000-0002-0134-2024>
 Diogo Souto  <https://orcid.org/0000-0002-7883-5425>
 Lyra Cao  <https://orcid.org/0000-0002-8849-9816>
 Kevin Covey  <https://orcid.org/0000-0001-6914-7797>
 Steven R. Majewski  <https://orcid.org/0000-0003-2025-3147>
 Cintia Martinez  <https://orcid.org/0000-0003-2745-8241>
 Philip S. Muirhead  <https://orcid.org/0000-0002-0638-8822>
 Marc Pinsonneault  <https://orcid.org/0000-0002-7549-7766>
 C. Allende Prieto  <https://orcid.org/0000-0002-0084-572X>
 Keivan G. Stassun  <https://orcid.org/0000-0002-3481-9052>

References

- Abdurro'uf, Accetta, K., Aerts, C., et al. 2022, *ApJS*, **259**, 35
- Afram, N., Reiners, A., & Berdyugina, S. V. 2009, in ASP Conf. Ser. 405, Solar Polarization 5: In Honor of Jan Stenflo, ed. S. V. Berdyugina, K. N. Nagendra, & R. Ramelli (San Francisco, CA: ASP), 527
- Astudillo-Defru, N., Delfosse, X., Bonfils, X., et al. 2017, *A&A*, **600**, A13
- Bailer-Jones, C. A. L., Rybizki, J., Fouesneau, M., Demleitner, M., & Andrae, R. 2021, *AJ*, **161**, 147
- Bakos, G., Noyes, R. W., Kovács, G., et al. 2004, *PASP*, **116**, 266
- Baraffe, I., Homeier, D., Allard, F., & Chabrier, G. 2015, *A&A*, **577**, A42
- Barnes, S. A. 2003, *ApJ*, **586**, 464
- Basri, G., & Marcy, G. W. 1994, *ApJ*, **431**, 844
- Basri, G., Marcy, G. W., & Valenti, J. A. 1992, *ApJ*, **390**, 622
- Belokurov, V., Penoyre, Z., Oh, S., et al. 2020, *MNRAS*, **496**, 1922
- Blanton, M. R., Bershad, M. A., Abolfathi, B., et al. 2017, *AJ*, **154**, 28
- Bowen, I. S., & Vaughan, A. H. J. 1973, *ApOpt*, **12**, 1430
- Bressan, A., Marigo, P., Girardi, L., et al. 2012, *MNRAS*, **427**, 127
- Cantat-Gaudin, T., Anders, F., Castro-Ginard, A., et al. 2020, *A&A*, **640**, A1
- Cao, L., & Pinsonneault, M. H. 2022, *MNRAS*, **517**, 2165
- Chabrier, G., Gallardo, J., & Baraffe, I. 2007, *A&A*, **472**, L17
- Choi, J., Dotter, A., Conroy, C., et al. 2016, *ApJ*, **823**, 102
- Covey, K. R., Agüeros, M. A., Law, N. M., et al. 2016, *ApJ*, **822**, 81
- Cristofari, P. I., Donati, J. F., Folsom, C. P., et al. 2023a, *MNRAS*, **522**, 1342

- Cristofari, P. I., Donati, J. F., Moutou, C., et al. 2023b, *MNRAS*, **526**, 5648
- Cui, X.-Q., Zhao, Y.-H., Chu, Y.-Q., et al. 2012, *RAA*, **12**, 1197
- Dahm, S. E. 2015, *ApJ*, **813**, 108
- Dotter, A., Chaboyer, B., Jevremović, D., et al. 2008, *ApJS*, **178**, 89
- Fang, X.-S., Zhao, G., Zhao, J.-K., & Bharat Kumar, Y. 2018, *MNRAS*, **476**, 908
- Feiden, G. A., Jones, J., & Chaboyer, B. 2015, Proc. 18th Cambridge Workshop on Cool Stars, Stellar Systems, and the Sun, ed. G. van Belle & H. C. Harris, 171
- Foreman-Mackey, D., Conley, A., Meierjürgen Farr, W., et al. 2013, emcee: The MCMC Hammer, Astrophysics Source Code Library, ascl:1303.002
- Gaia Collaboration, Vallenari, A., Brown, A. G. A., et al. 2023, *A&A*, **674**, A1
- García Pérez, A. E., Allende Prieto, C., Holtzman, J. A., et al. 2016, *AJ*, **151**, 144
- Gunn, J. E., Siegmund, W. A., Mannery, E. J., et al. 2006, *AJ*, **131**, 2332
- Gustafsson, B., Edvardsson, B., Eriksson, K., et al. 2008, *A&A*, **486**, 951
- Hahlin, A., & Kochukhov, O. 2022, *A&A*, **659**, A151
- Hahlin, A., Kochukhov, O., Alecian, E., Morin, J. & BinaMiCS Collaboration 2021, *A&A*, **650**, A197
- Hahlin, A., Kochukhov, O., Rains, A. D., et al. 2023, *A&A*, **675**, A91
- Han, E., López-Valdivia, R., Mace, G. N., & Jaffe, D. T. 2023, *AJ*, **166**, 4
- Harris, C. R., Millman, K. J., van der Walt, S. J., et al. 2020, *Natur*, **585**, 357
- Hartman, J. D., Bakos, G. Á, Kovács, G., & Noyes, R. W. 2010, *MNRAS*, **408**, 475
- Hawley, S. L., Davenport, J. R. A., Kowalski, A. F., et al. 2014, *ApJ*, **797**, 121
- Heyl, J., Caiazzo, I., & Richer, H. B. 2022, *ApJ*, **926**, 132
- Howell, S. B., Sobeck, C., Haas, M., et al. 2014, *PASP*, **126**, 398
- Hubeny, I., & Lanz, T. 2011, Synspec: General Spectrum Synthesis Program, Astrophysics Source Code Library, ascl:1109.022
- Hunter, J. D. 2007, *CSE*, **9**, 90
- Jackson, R. J., Deliyannis, C. P., & Jeffries, R. D. 2018, *MNRAS*, **476**, 3245
- Jackson, R. J., Jeffries, R. D., Deliyannis, C. P., Sun, Q., & Douglas, S. T. 2019, *MNRAS*, **483**, 1125
- Jackson, R. J., Jeffries, R. D., Randich, S., et al. 2016, *A&A*, **586**, A52
- Jaehnig, K., Somers, G., & Stassun, K. G. 2019, *ApJ*, **879**, 39
- Jeffers, S. V., Schöfer, P., Lamert, A., et al. 2018, *A&A*, **614**, A76
- Johns-Krull, C. M. 2007, *ApJ*, **664**, 975
- Johns-Krull, C. M., & Valenti, J. A. 1996, *ApJL*, **459**, L95
- Johns-Krull, C. M., & Valenti, J. A. 2000, in ASP Conf. Ser. 198, Stellar Clusters and Associations: Convection, Rotation, and Dynamos, ed. R. Pallavicini, G. Micela, & S. Sciortino (San Francisco, CA: ASP), 371
- Johns-Krull, C. M., Valenti, J. A., & Saar, S. H. 2004, *ApJ*, **617**, 1204
- Kawaler, S. D. 1988, *ApJ*, **333**, 236
- Kesseli, A. Y., Muirhead, P. S., Mann, A. W., & Mace, G. 2018, *AJ*, **155**, 225
- Kochukhov, O. 2016, in Cartography of the Sun and the Stars, ed. J.-P. Rozelot & C. Neiner, Vol. 914 (Berlin: Springer), 177
- Kochukhov, O. 2021, *A&ARv*, **29**, 1
- Kochukhov, O., Heiter, U., Piskunov, N., et al. 2009, in AIP Conf. Ser. 1094, Cool Stars, Stellar Systems, and the Sun, ed. E. Stempels (Melville, NY: AIP), 124
- Kochukhov, O., & Lavail, A. 2017, *ApJL*, **835**, L4
- Kochukhov, O., Makaganiuk, V., & Piskunov, N. 2010, *A&A*, **524**, A5
- Kochukhov, O., Piskunov, N., Valenti, J., & Johns-Krull, C. 2001, in ASP Conf. Ser. 248, Magnetic Fields Across the Hertzsprung–Russell Diagram, ed. G. Mathys, S. K. Solanki, & D. T. Wickramasinghe (San Francisco, CA: ASP), 219
- Kochukhov, O., & Reiners, A. 2020, *ApJ*, **902**, 43
- Kochukhov, O., & Shulyak, D. 2019, *ApJ*, **873**, 69
- Kupka, F., Piskunov, N., Ryabchikova, T. A., Stempels, H. C., & Weiss, W. W. 1999, *A&AS*, **138**, 119
- Lasker, B. M., Lattanzi, M. G., McLean, B. J., et al. 2008, *AJ*, **136**, 735
- Lavail, A., Kochukhov, O., & Hussain, G. A. J. 2019, *A&A*, **630**, A99
- Law, N. M., Kulkarni, S. R., Dekany, R. G., et al. 2009, *PASP*, **121**, 1395
- Lodieu, N., Pérez-Garrido, A., Smart, R. L., & Silvotti, R. 2019, *A&A*, **628**, A66
- Majewski, S. R., Schiavon, R. P., Frinchaboy, P. M., et al. 2017, *AJ*, **154**, 94
- Mann, A. W., Feiden, G. A., Gaidos, E., Boyajian, T., & von Braun, K. 2015, *ApJ*, **804**, 64
- Mann, A. W., Feiden, G. A., Gaidos, E., Boyajian, T., & von Braun, K. 2016, *ApJ*, **819**, 87
- Micela, G., Sciortino, S., Harnden, F. R. J., et al. 1999, *A&A*, **341**, 751
- Micela, G., Sciortino, S., Kashyap, V., Harnden, F. R. J., & Rosner, R. 1996, *ApJS*, **102**, 75
- Micela, G., Sciortino, S., Vaiana, G. S., et al. 1990, *ApJ*, **348**, 557
- Muirhead, P. S., Dressing, C. D., Mann, A. W., et al. 2018, *AJ*, **155**, 180
- Newton, E. R., Irwin, J., Charbonneau, D., Berta-Thompson, Z. K., & Dittmann, J. A. 2016, *ApJL*, **821**, L19
- Newton, E. R., Irwin, J., Charbonneau, D., et al. 2017, *ApJ*, **834**, 85
- Nguyen, C. T., Costa, G., Girardi, L., et al. 2022, *A&A*, **665**, A126
- Nidever, D. L., Holtzman, J. A., Allende Prieto, C., et al. 2015, *AJ*, **150**, 173
- Núñez, A., & Agüeros, M. A. 2016, *ApJ*, **830**, 44
- Perryman, M. A. C., Brown, A. G. A., Lebreton, Y., et al. 1998, *A&A*, **331**, 81
- Phan-Bao, N., Lim, J., Donati, J.-F., Johns-Krull, C. M., & Martín, E. L. 2009, *ApJ*, **704**, 1721
- Piskunov, N. E., Kupka, F., Ryabchikova, T. A., Weiss, W. W., & Jeffery, C. S. 1995, *A&AS*, **112**, 525
- Plez, B. 2012, Turbospectrum: Code for spectral synthesis, Astrophysics Source Code Library, ascl:1205.004
- Pouilly, K., Kochukhov, O., Kóspál, Á., et al. 2023, *MNRAS*, **518**, 5072
- Rau, A., Kulkarni, S. R., Law, N. M., et al. 2009, *PASP*, **121**, 1334
- Rebull, L. M., Stauffer, J. R., Bouvier, J., et al. 2016, *AJ*, **152**, 114
- Reid, I. N., & Gizis, J. E. 1997, *AJ*, **113**, 2246
- Reiners, A., Basri, G., & Christensen, U. R. 2009, *ApJ*, **697**, 373
- Reiners, A., Joshi, N., & Goldman, B. 2012, *AJ*, **143**, 93
- Reiners, A., Shulyak, D., Käpylä, P. J., et al. 2022, *A&A*, **662**, A41
- Saar, S. H. 1994, in IAU Symp. 154, Infrared Solar Physics, ed. D. M. Rabin, J. T. Jefferies, & C. Lindsey (Cambridge: Cambridge Univ. Press), 493
- Saar, S. H. 1996, in IAU Symp. 176, Stellar Surface Structure ed. K. G. Strassmeier & J. L. Linsky (Dordrecht: Kluwer), 237
- Saar, S. H., & Linsky, J. L. 1985, *ApJL*, **299**, L47
- Salpeter, E. E. 1955, *ApJ*, **121**, 161
- Shulyak, D., Reiners, A., Engeln, A., et al. 2017, *NatAs*, **1**, 0184
- Shulyak, D., Reiners, A., Nagel, E., et al. 2019, *A&A*, **626**, A86
- Shulyak, D., Reiners, A., Seemann, U., Kochukhov, O., & Piskunov, N. 2014, *A&A*, **563**, A35
- Shulyak, D., Seifahrt, A., Reiners, A., Kochukhov, O., & Piskunov, N. 2011, *MNRAS*, **418**, 2548
- Skrutskie, M. F., Cutri, R. M., Stiening, R., et al. 2006, *AJ*, **131**, 1163
- Skumanich, A. 1972, *ApJ*, **171**, 565
- Smith, V. V., Bizyaev, D., Cunha, K., et al. 2021, *AJ*, **161**, 254
- Soderblom, D. R., Laskar, T., Valenti, J. A., Stauffer, J. R., & Rebull, L. M. 2009, *AJ*, **138**, 1292
- Somers, G., Cao, L., & Pinsonneault, M. H. 2020, *ApJ*, **891**, 29
- Souto, D., Cunha, K., García-Hernández, D. A., et al. 2017, *ApJ*, **835**, 239
- Souto, D., Cunha, K., Smith, V. V., et al. 2020, *ApJ*, **890**, 133
- Souto, D., Cunha, K., & Smith, V. V. 2021, *ApJ*, **917**, 11
- Stassun, K. G., Kratter, K. M., Scholz, A., & Dupuy, T. J. 2012, *ApJ*, **756**, 47
- Stauffer, J. R., Caillault, J. P., Gagne, M., Prosser, C. F., & Hartmann, L. W. 1994, *ApJS*, **91**, 625
- Stauffer, J. R., Hartmann, L. W., Fazio, G. G., et al. 2007, *ApJS*, **172**, 663
- Stelzer, B., Neuhäuser, R., & Hambaryan, V. 2000, *A&A*, **356**, 949
- Stift, M. J., & Leone, F. 2003, *A&A*, **398**, 411
- Wanderley, F., Cunha, K., Souto, D., et al. 2023, *ApJ*, **951**, 90
- Wang, S., & Chen, X. 2019, *ApJ*, **877**, 116
- Wilson, J. C., Hearty, F. R., Skrutskie, M. F., et al. 2019, *PASP*, **131**, 055001
- Wright, N. J., Drake, J. J., Mamajek, E. E., & Henry, G. W. 2011, *ApJ*, **743**, 48
- Yang, H., & Johns-Krull, C. M. 2011, *ApJ*, **729**, 83
- Yang, H., Johns-Krull, C. M., & Valenti, J. A. 2008, *AJ*, **136**, 2286
- Zacharias, N., Finch, C. T., Girard, T. M., et al. 2012, *yCat*, **1/322A**